Magnetocaloric effect due to spin reorientation in the crystalline electrical field: Theory applied to $DyAl_2$

P. J. von Ranke,[1,*] N. A. de Oliveira,[1] D. C. Garcia,[1] V. S. R. de Sousa,[1] V. A. de Souza,[1] A. Magnus G. Carvalho,[2] S. Gama,[2] and M. S. Reis[3]

[1]*Instituto de Física, Universidade do Estado do Rio de Janeiro (UERJ), Rua São Francisco Xavier, 524, 20550-013 Rio de Janeiro, Brazil*

[2]*Instituto de Física "Gleb Wataghin," Universidade Estadual de Campinas (UNICAMP), C.P. 6165, Campinas 13, 083-970 São Paulo, Brazil*

[3]*CICECO, Universidade de Aveiro, 3810-193 Aveiro, Portugal*

(Received 17 January 2007; revised manuscript received 17 March 2007; published 17 May 2007)

We report a way of obtaining the magnetocaloric effect due to the crystal electrical-field quenching of the total angular momentum in a magnetic system where a strong spin reorientation is present. The theoretical model is applied to $DyAl_2$ and the results predict a considerable magnetic entropy change by rotating a single crystal in a fixed magnetic field. The obtained temperature and magnetic-field dependencies of the magnetization component along the ⟨111⟩-crystallographic direction are in good agreement with the recently reported experimental data.

DOI: 10.1103/PhysRevB.75.184420 PACS number(s): 75.30.Sg, 75.10.Dg, 75.20.En

I. INTRODUCTION

Intensive efforts have been concentrated in the study of the magnetocaloric effect (MCE) since the discovery[1] of the giant magnetocaloric effect in $Gd_5(Si_xGe_{1-x})_4$ in a broad temperature range, from cryogenic temperature to room temperature, by changing the silicon concentration for $x \leqslant 0.5$. From a practical point of view, this discovery attracted, immediately, much attention due to the potential application of the $Gd_5(Si_xGe_{1-x})_4$ compounds as refrigerant materials to work in magnetic refrigerator,[2,3] specially around room temperature, which has high commercial and ecological interest. The origin of the giant MCE was experimentally investigated and ascribed to the coupled order-disorder magnetic and crystallographic phase transitions in a first-order process. Other giant magnetocaloric materials were discovered since then, such as $MnFeP_{0.45}As_{0.55}$,[4] $MnAs_{1-x}Sb_x$,[5,6] and $La(Fe_{1-x}Si_x)_{13}$.[7,8] The MCE is characterized by the two main quantities, namely, the isothermal magnetic entropy change ΔS_{iso} and the adiabatic temperature change ΔT_{ad} which are observed upon magnetic-field changes. Theoretical models in which the magnetoelastic interaction is considered, through the exchange interaction dependence of the lattice deformation, were successfully[9–11] applied to the giant MCE in $Gd_5(Si_xGe_{1-x})_4$, $MnFeP_{0.45}As_{0.55}$, and $MnAs_{1-x}Sb_x$.

More recently, the so-called colossal MCE was discovered in MnAs under hydrostatic pressure.[12] The colossal MCE occurs when the isothermal entropy change in a given material is greater than the maximum magnetic entropy change, i.e., $\Delta S > \Delta S_{mag}^{max} = R \ln(2J+1)$, where R is the gas constant and J is the total angular momentum of the magnetic free ion. The origin of the colossal MCE was theoretically investigated[13] considering the lattice entropy dependence on the crystalline cell deformation through the magnetoelastic interaction. Therefore, the extra entropy change which leads to the colossal MCE was ascribed to the lattice entropy contribution, in an isothermic process. The theoretical model[14] constructed to explain the colossal MCE reproduces satisfactorily the results of ΔS vs T in MnAs under hydrostatic pressure.

The full crystallographic investigations of the magnetocaloric materials are of fundamental importance to highlight the proper configuration of the interactions to be considered in theoretical models. For example, the crystalline electrical-field (CEF) interaction can reveal several aspects associated with the anisotropy of the magnetocaloric effect since the magnetocaloric quantities, ΔS_{iso} and ΔT_{ad}, depend on the magnetic-field direction in relation to the crystallographic axes. A detailed theoretical investigation, considering the CEF interaction in the paramagnetic $PrNi_5$ compound, predicted the anomalous MCE (this paramagnetic material shows an increase of magnetic entropy when submitted to applied magnetic field which leads to a cooling in the presence of magnetic field.[15,16] Also, the anomalous peaks in ΔS_{iso} experimentally observed in $(Dy_{1-x}Er_x)Al_2$ (Ref. 17) and the anomalous MCE in YbAs (associated with the giant quadrupolar interaction)[18] were satisfactorily explained in the framework of the CEF model as well. Recently, experimental data of ΔS_{iso} in $DyAl_2$ showed the existence of an anomalous[19] MCE when the magnetic field is applied in a noneasy magnetic direction, namely, the ⟨111⟩ direction, as previously theoretically predicted.[20]

It is well known that in several systems, the rare-earth magnetic ions have a reduction on the total orbital magnetic moment due to the CEF, the so-called CEF-quenching effect. The basic principle of the CEF quenching is due to the inhomogeneous electric field created by the surrounding charges on the magnetic ions. Without this inhomogeneous electric field, the nuclear central fields lead, in quantum theory, to the conservation of only one component of angular momentum (usually taken as L_z), so in the presence of an inhomogeneous electric field the L_z component will no longer be a constant and can average to a reduced value, decreasing the mean value of the total angular momentum of the magnetic ion. It should be noted that the CEF quenching of the magnetic moment is dependent on the orientation of

the magnetic moment (and therefore magnetization) in relation to the crystallographic axes. In this way, an applied magnetic field in anisotropic magnetic materials, in a noneasy magnetic direction, can reorient the magnetization, changing its intensity. When the reorientation occurs, especially in a first-order process, a strong change in magnetization intensity, due to the CEF quenching, is expected. This quenching originates a ΔS_{iso} (in fixed external magnetic field) due to a rotation process, which we will call from now on the anisotropic MCE. We stress that the anisotropic MCE is a pure quantum mechanical effect, since in classical theory the intensity of the magnetization vector does not change in the alignment process with the external magnetic field. In this paper, we report the anisotropic MCE in $DyAl_2$. The magnetic state equation is obtained from a model Hamiltonian which includes the Zeeman, exchange, and CEF interactions. The magnetic state equation is solved considering a three-dimensional self-consistent numerical procedure, in the magnetization vector components, which is an extension of the two-dimensional self-consistent procedure adopted by Bak.[21]

II. THEORY

The magnetic properties of the $DyAl_2$ compound can be described starting from a model Hamiltonian which includes the following interactions: (1) cubic crystalline electrical-field interaction, in the approach of the point-charge model;[22] (2) the exchange interaction, in the molecular-field assumption; and (3) the Zeeman interaction. The Hamiltonian is given by

$$\hat{H} = \hat{H}_{CEF} + \hat{H}_{mag}, \tag{1}$$

where

$$\hat{H}_{CEF} = W\left[\frac{X}{F_4}(O_4^0 + 5O_4^4) + \frac{(1-|X|)}{F_6}(O_6^0 - 21O_6^4)\right] \tag{2}$$

and

$$\hat{H}_{mag} = -g\mu_B(\vec{H} + \lambda\vec{M})\cdot\vec{J}. \tag{3}$$

The above vector relation is conveniently written in Cartesian component representation and we obtain

$$\hat{H}_{mag} = -g\mu_B[(H\cos\alpha + \lambda M_x)J_x + (H\cos\beta + \lambda M_y)J_y + (H\cos\gamma + \lambda M_z)J_z]. \tag{4}$$

Relation (2) is the single-ion CEF Hamiltonian written in the Lea-Leask-Wolf representation,[23] where W gives the CEF energy scale and X $(-1<X<1)$ gives the relative contributions of the fourth and sixth degrees in O_n^m Stevens' equivalent operators.[24] The dimensionless constants F_4 and F_6 for rare-earth ions were tabulated in Ref. 23 and have the following values for Dy: $F_4=60$ and $F_6=13\,860$.

Relation (3) is the single-ion magnetic Hamiltonian, taken in the molecular-field approximation, where g is the Lande factor, μ_B is the Bohr magneton, and H is the intensity of the applied magnetic field on an arbitrary direction forming the angles α, β, and γ with the cubic crystallographic axes x, y, and z, respectively (z was considered as the quantization direction). The three components of the magnetization and total angular momentum vectors are M_k and J_k $(k=x,y,z)$, respectively. The intensity of the magnetization M and the component of the magnetization vector M_h along the applied magnetic-field direction are

$$M = \sqrt{M_x^2 + M_y^2 + M_z^2}, \tag{5}$$

$$M_h = \cos(\alpha)M_x + \cos(\beta)M_y + \cos(\gamma)M_z. \tag{6}$$

The components of the magnetization vector are obtained by the mean thermodynamic values of the magnetic moments,

$$M_k = g\mu_B \frac{\sum_j \langle E_j|J_k|E_j\rangle \exp(-E_j/k_BT)}{\sum_j \exp(-E_j/k_BT)}. \tag{7}$$

In this relation, E_j and $|E_j\rangle$ are the energy eigeinvalues and eigeinvectors of Hamiltonian (1). It should be observed that E_j and $|E_j\rangle$ depend on the three magnetization vector components. Therefore, in order to obtain the magnetization components from relation (7), it is necessary to solve a *three-dimensional* self-consistent problem.

The total entropy S of the $DyAl_2$ compound can be decoupled in the three main contributions and is given by

$$S(H,T) = S_{mag}(H,T) + S_{lat}(T) + S_{el}(T), \tag{8}$$

where S_{mag} is the magnetic contribution which can be obtained from the general relation

$$S_{mag}(T,H) = \left(\frac{1}{T}\right)\frac{\sum_j E_j \exp(-E_j/k_BT)}{\sum_j \exp(-E_j/k_BT)} + k_B \ln\left[\sum_j \exp(-E_j/k_BT)\right]. \tag{9}$$

The temperature and field dependencies of the above magnetic entropy are not trivial, since for a given pair (T,H), the $M_k=M_k(T,H,M_x,M_y,M_z)$ must be determined self-consistently in order to obtain the proper set of energy eigeinvalues E_j from the total Hamiltonian, relation (1), to update relation (9).

The lattice entropy can be calculated using the Debye relation

$$S_{lat} = -3R\ln[1-\exp(-\Theta_D/T)] + 12R\left(\frac{T}{\Theta_D}\right)^3 \int_0^{\Theta_D/T} \frac{x^3 dx}{\exp(x)-1}, \tag{10}$$

where R is the gas constant and Θ_D is the Debye temperature.

The electronic entropy can be obtained from the standard relation

$$S_{\mathrm{el}} = \bar{\gamma}T, \tag{11}$$

where $\bar{\gamma}$ is the linear electronic heat capacity coefficient.

The magnetocaloric potential, i.e., the isothermal entropy change ΔS_{iso} and the adiabatic temperature change ΔT_{ad}, that occur for changes in the external magnetic field are obtained from relation (8), plotting the total entropy versus temperature with and without external magnetic field and computing the isothermal and adiabatic differences from this pair of curves,

$$\Delta S_{iso}(T,H) = S(T,H=0) - S(T,H), \tag{12}$$

$$\Delta T_{ad} = T(T,H) - T(T,H=0). \tag{13}$$

It should be noted that the above quantities can be strongly dependent on the magnetic-field direction in anisotropic magnetic materials. In this way, we define the isothermic and adiabatic anisotropic-MCE quantities as

$$\Delta S_{iso}[\alpha_e,\beta_e,\gamma_e][\alpha,\beta,\gamma] = S(T,H,\alpha_e,\beta_e,\gamma_e) - S(T,H,\alpha,\beta,\gamma), \tag{14}$$

$$\Delta T_{ad}[\alpha_e,\beta_e,\gamma_e][\alpha,\beta,\gamma] = T(T,H,\alpha_e,\beta_e,\gamma_e) - T(T,H,\alpha,\beta,\gamma). \tag{15}$$

In these relations, the set $(\alpha_e,\beta_e,\gamma_e)$ represents the angles formed between the applied magnetic-field vector (in easy magnetic direction) and the Cartesian axes x, y, and z, respectively. The set (α,β,γ) represents the angles formed between the applied magnetic-field vector when in an arbitrary direction in relation to the Cartesian axes x, y, and z, respectively. In bracket form $[\alpha,\beta,\gamma]$, the usual crystallographic representation is considered, e.g., when the magnetic field is applied in the cubic diagonal direction $(\alpha,\beta,\gamma) = [\tan^{-1}(\sqrt{2}),\tan^{-1}(\sqrt{2}),\tan^{-1}(\sqrt{2})] \Rightarrow [\alpha,\beta,\gamma] = [111]$. In our case, considered in this work, the anisotropic MCE comes from the CEF anisotropy.

III. APPLICATION TO $DyAl_2$ AND DISCUSSION

The model parameters for $DyAl_2$ are $W=-0.0111$ meV, $X=0.3$, and $\lambda=41.6$ T^2/meV and were fitted to the experimental results for M_h. In this work, we consider the cubic crystalline axes of $DyAl_2$ oriented in the Cartesian axes in such a way that the quantization axis, i.e., z-[001], is considered in the easy magnetic direction of $DyAl_2$. Figure 1 shows the components of magnetization M_h versus magnetic field applied along the following directions: [001]-easy direction, [101], [111], and [100] at $T=4.2$ K. The solid curves are the theoretical results and the symbols represent the experimental data available in literature.[25] It is worth noticing that our model, discussed above, permits the calculation of the M_h along any cubic crystallographic direction where the magnetic field is applied. For example, the M_h for magnetic field applied in the cubic diagonal direction is obtained entering with $\cos\alpha=\cos\beta=\cos\gamma=\sqrt{3}/3$ in relations (4) and (6) and solving the self-consistent problem for the three magnetization components. As shown in Fig. 1, there are discontinuous changes in the $M_h^{[111]}$ and $M_h^{[100]}$ components at critical magnetic fields $H_R=5.75$ T and $H_R=6.13$ T. These discontinuities are due to the spin reorientation which occurs as first-order phase-transition processes. The $M_h^{[100]}$ component starts from zero value at $H=0$ T since the easy magnetic direction was considered along the [001] direction. In the same way, $M_h^{[010]}$ starts from zero at $H=0$ T (not shown in this work) which confirm that the CEF parameters, X and W, lead to the easy magnetic direction along the cubic z axis in our referential frame.

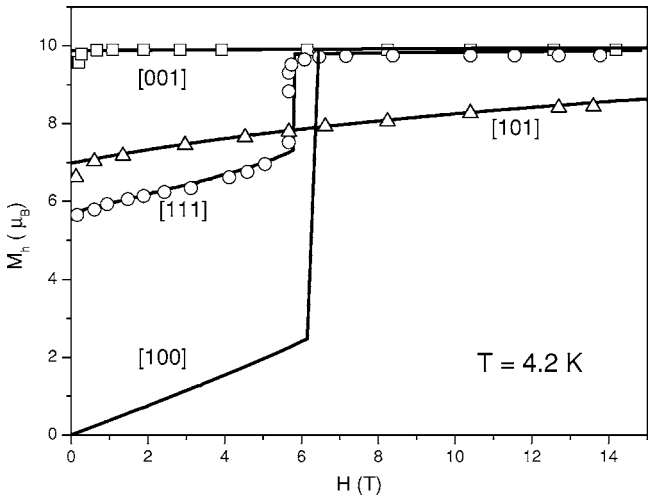

FIG. 1. The magnetization component along the magnetic-field directions, indicated in the bracket, versus applied magnetic field calculated at $T=4.2$ K. The symbols represent the experimental data for $DyAl_2$.

Figure 2 shows the $M_h^{[100]}$ versus H for different temperature values, namely, $T=4.2$, 10, 20, and 30 K. The effect of increasing temperature is to decrease the reorientation critical field H_R, since the thermal energy acts in a contrary way of anisotropic energy; the directional spin freedom increases with temperature. Figure 3 shows the $M_h^{[00\bar{1}]}$ versus H for different temperature values. It should be noted that for $H=0$ T, the magnetization values are negative, as expected, since the magnetic field is applied along the

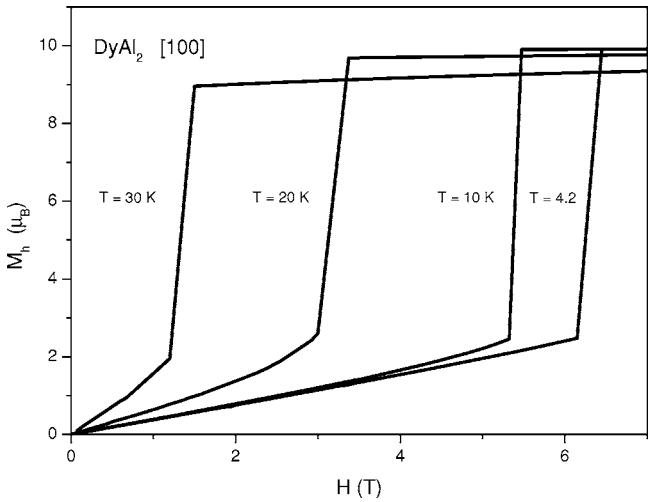

FIG. 2. The magnetization component along the magnetic-field direction [100] versus applied magnetic-field intensity calculated at $T=4.2$ K, $T=10$ K, $T=20$ K, and $T=30$ K for $DyAl_2$.

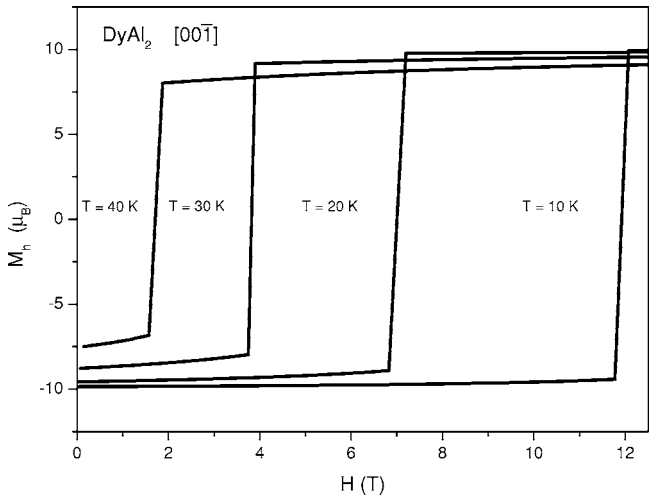

FIG. 3. The magnetization component along the magnetic-field direction [00$\bar{1}$] versus applied magnetic-field intensity calculated at $T=10$ K, $T=20$ K, $T=30$ K, and $T=40$ K for $DyAl_2$.

[00$\bar{1}$]-crystallographic direction which is opposite to the easy magnetic direction [001]. Therefore, in order to flip the magnetization in the applied magnetic-field direction, a higher magnetic-field intensity is necessary. For temperatures $T=10$, 20, and 30 K, the intensities of the magnetic field, i.e., the reorientation fields, are $H_R^{[100]}=5.35$, 3.01, and 1.26 T which are lower than the $H_R^{[00\bar{1}]}=11.76$, 6.85, and 3.78 T for the same set of temperature values, respectively (see Figs. 2 and 3). It is worth noticing that even for $H>H_R$, the magnetization M aligned with the applied magnetic field is not yet saturated, as shown in Figs. 2 and 3 for the higher temperatures in the M_h vs H curves considered.

Figure 4 shows the magnetic-field dependence of the M_h and M calculated for the magnetic field applied in the [00$\bar{1}$] direction at $T=40$ K. It should be noted the completely different behavior of the M vs H curve [obtained from relation (5)] compared with the M_h one. Although the magnetization component M_h along the magnetic field increases due to the rotation process, the modulus of the magnetization M decreases with applied field until the H_R is achieved. For $H>H_R$, obviously, we have $M_h=M$ since the rotation process is fully completed. The decrease in M is a pure quantum mechanics effect, the so-called CEF quenching, which depends on the magnetic-moment orientation. When the magnetic moment is rotated in a crystal, a different charge environment distribution acts on the magnetic moment (in orbital momentum contribution), leading to different quenching of the CEF interaction on the magnetic ion. In a picture description, the magnetic moment should be reduced to escape from the potential well of the magnetocrystalline anisotropy, which holds the magnetic moment fixed in the easy magnetic direction. From classical theory, only a rotation of the magnetic moment occurs in an alignment magnetic-field process. The inset of Fig. 4 shows the change in the modulus of the magnetization vector around the critical reorientation field (a change in magnetization ΔM of about 15% of the M value is predicted to occur at H_R) and its influence on the magnetocaloric effect will be discussed below.

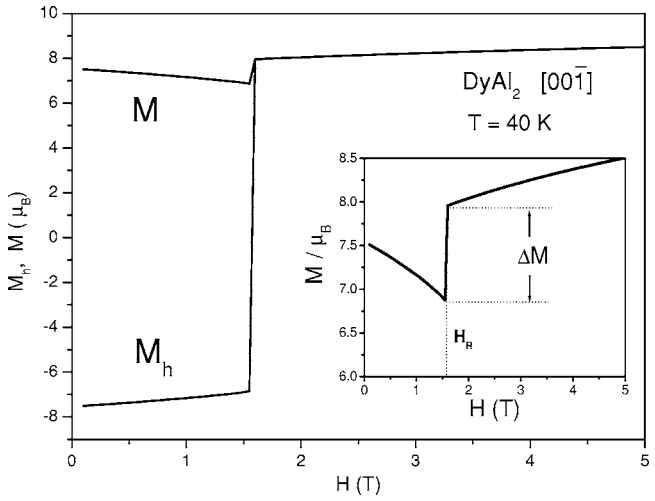

FIG. 4. The magnetization component, M_h, along the magnetic-field direction [00$\bar{1}$] and the magnetization intensity, M, versus applied magnetic-field intensity calculated at $T=40$ K. The inset shows the magnetization changes due to the spin reorientation process at $H_R=1.6$ T.

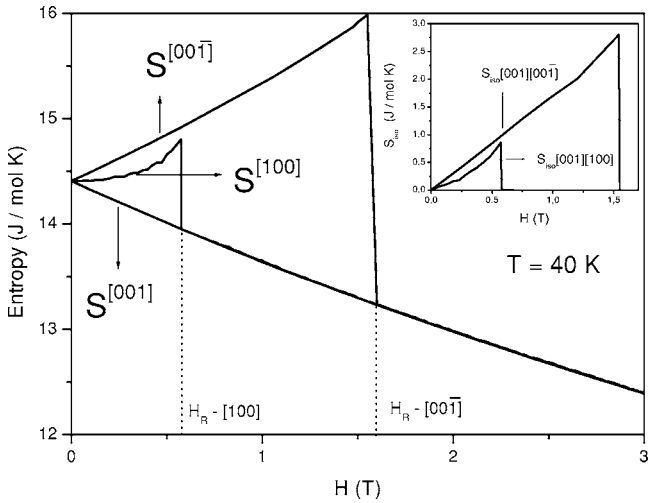

FIG. 5. The magnetic entropy in $DyAl_2$ versus magnetic field applied in three directions: [001]-easy direction, [100], and [00$\bar{1}$] calculated at $T=40$ K. The reorientation magnetic fields are shown by the dotted lines. The inset shows the anisotropic MEC.

Figure 5 shows the magnetic-field dependence of the magnetic entropy calculated from relation (9) considering the following magnetic-field directions: [001], [100], and [00$\bar{1}$] at $T=40$ K. As expected, a continuous and decreasing curve appears when the intensity of the magnetic field increases in the easy magnetic [001] direction. On the other hand, when the magnetic field is applied on the [100] and [00$\bar{1}$] directions, continuous increases are observed in the entropy curves from zero to the corresponding reorientation fields, namely, $H_R=0.58$ T (for [100] and $H_R=1.57$ T (for [00$\bar{1}$]). At the reorientation fields, an abrupt change occurs in both $S_{mag}^{[100]}$ and $S_{mag}^{[00\bar{1}]}$ magnetic entropy curves, and for $H>H_R$ all the entropy curves relapse on the entropy curve $S_{mag}^{[001]}$. The

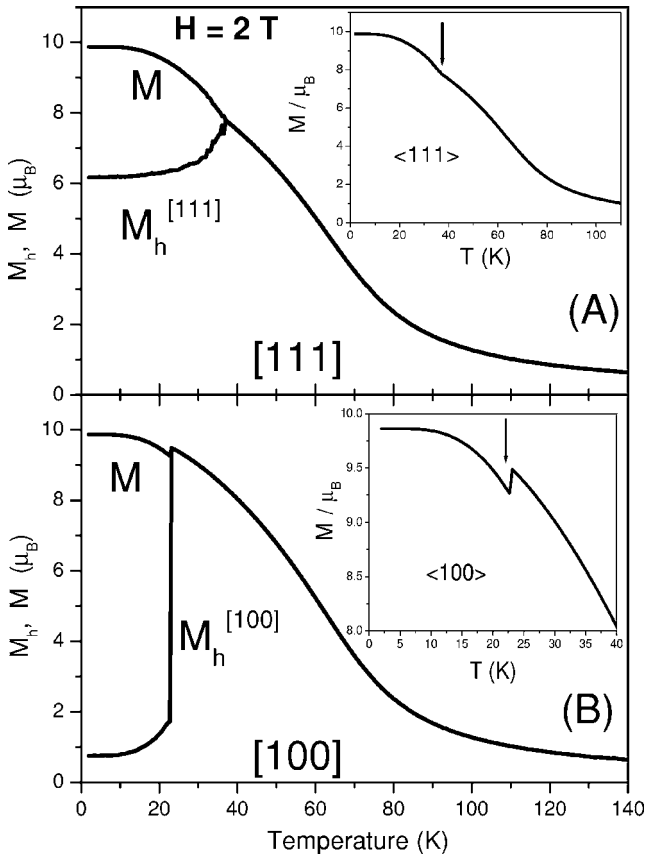

FIG. 6. The magnetization component, M_h, along the magnetic-field directions [111] (A) and [100] (B) and the magnetization intensity, M, versus T in $DyAl_2$ calculated at $H=2$ T. The insets show the detail of M versus T around the reorientation spin temperatures indicated by the arrows.

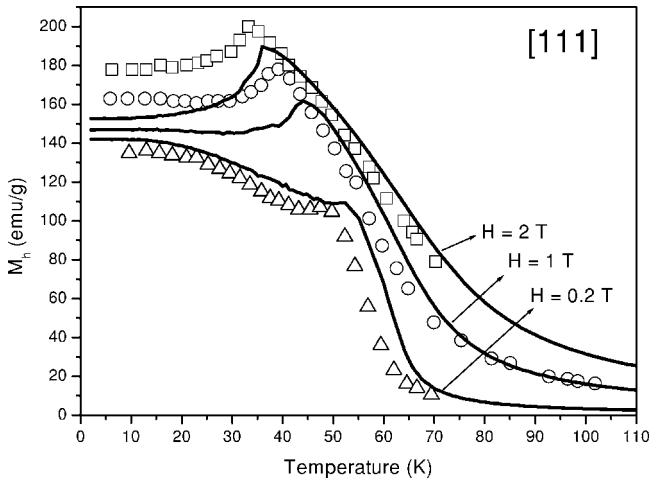

FIG. 7. The magnetization component curves, M_h, along the magnetic-field direction [111] versus temperature for three values of applied magnetic field $H=0.2$ T, $H=1$ T, and $H=2$ T. The solid curves are the theoretical results and the symbols represent the experimental data for $DyAl_2$ from (Ref. 19).

anomalous increase in magnetic entropy for increasing magnetic-field intensity below H_R can be understood by analyzing the M versus H curve plotted in Fig. 4. The magnetization (order parameter) decreases as the magnetic field increases in the interval $0<H<H_R$, leading to the anomalous entropy increase in the same magnetic-field interval (see M vs H in Fig. 4 and $S_{mag}^{[00\bar{1}]}$ vs H in Fig. 5). Above the reorientation magnetic field, both magnetization and entropy curves, calculated for the noneasy magnetic direction, present the same behavior as the magnetization and entropy curves calculated for the applied magnetic field in the easy direction. In this way, the predicted anomalous increase in the magnetic entropy, calculated in this work for the [100] and $[00\bar{1}]$ directions, comes from the anisotropy through the CEF quenching of the total angular momentum. It must be highlighted that changes in the magnetic entropy can be obtained at a fixed external magnetic-field intensity by changing its direction in relation to the crystallographic axes. Therefore, it is interesting to introduce the concept of anisotropic MCE as stated in relations (14) and (15). In these relations, the usual magnetocaloric quantities, ΔS_{iso} and ΔT_{ad}, are extended to include the anisotropy effect, i.e., under a fixed external magnetic-field intensity these quantities depend on the magnetic-field direction in the crystallographic referential frame. In the present work, the origin of the anisotropic MCE (predicted for the $DyAl_2$ compound) comes from the change in the magnetization due to the CEF-quenching effect. Nevertheless, other anisotropic microscopic mechanisms responsible for the directional magnetic-field influence on the quantities ΔS_{iso} and ΔT_{ad} can also be investigated within the concept of anisotropic MCE described above. The inset in Fig. 5 shows the ΔS_{iso} versus magnetic field for the two cases considered in Fig. 5.

Figure 6(a) shows the temperature dependence of the magnetization M and the magnetization component, $M_h^{[111]}$, along the applied magnetic field $H=2$ T oriented in the [111]-crystallographic direction. As the temperature increases, the component $M_h^{[111]}$ also increases until a critical temperature $T_R=36.5$ K. The magnetization M decreases with the increasing of the temperature and for $T_R \geqslant 36.5$ K we have $M=M_h^{[111]}$, i.e., the two curves are coincident. In this way, $T_R=36.5$ K is the critical spin reorientation temperature. The spin reorientation process temperature can be described in the following way: the role of the anisotropy energy due to the CEF environment is to hold the magnetization in the easy magnetic direction and the applied magnetic field, in a noneasy magnetic direction, tends to rotate the magnetization vector from the easy magnetic direction to the applied magnetic-field direction. For a fixed magnetic-field intensity (less than the critical spin reorientation field H_R discussed above), the increase of temperature (thermal energy) leads to liberation of the anisotropy energy and therefore a reorientation process occurs which is fully completed at T_R. The inset of Fig. 6(a) shows the details of M versus T around the reorientation process and the arrows indicate the discontinuity of M at T_R.

Figure 6(b) shows the temperature dependence of the M and its component $M_h^{[100]}$ along applied magnetic field oriented in the [100] direction and with the intensity of $H=2$ T. We can observe that the spin reorientation temperature is $T_R=23$ K for the [100] direction which is lower than the

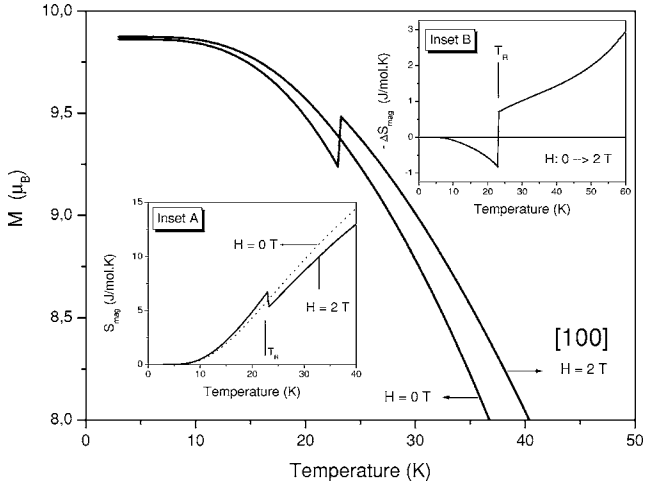

FIG. 8. The magnetization versus temperature in $H=0$ T (dotted curve) and in $H=2$ T along the [100] direction (full curve); Inset (A) shows the magnetic entropy in $H=0$ T (dotted curve) and in $H=2$ T (full curve); the arrow indicates the spin reorientation temperature. Inset (B) shows the ΔS_{mag} vs T around the reorientation temperature.

one obtained for the [111] direction. Therefore, in general, the spin reorientation temperature depends on the magnetic-field direction as well as the magnetic-field intensity (as will be discussed below in the context of Fig. 7). At low temperature, the value of $M_h^{[100]}=0.75\mu_B$ is calculated and it is worth noticing that this value depends on the magnetic-field direction as well as the magnetic-field intensity. In particular, for zero magnetic field, we have $M_h^{[100]}=0$ since the easy magnetic direction is along the [001]-crystallographic direction, as discussed above. For $H=2$ T, $M_h^{[100]}$ increases smoothly in the temperature interval $0<T<23$ K and at $T_R=23$ K a jump occurs in the $M_h^{[100]}$, leading to a first-order spin reorientation transition. The magnetization intensity, M, also presents a strong discontinuity at T_R which can be better noted in the inset of Fig. 6(b).

Figure 7 shows the temperature dependence of the $M_h^{[111]}$ for applied magnetic fields $H=0.2$, 1, and 2 T. The solid lines represent our theoretical results and the symbols represent the experimental data.[19] We stress the importance of the three-dimensional mean-field model, considered in this paper, in order to obtain the simultaneous convergence of the three magnetization components used in the calculation of $M_h^{[111]}$ for each magnetic-field intensity and temperature. It should be noted that peaks in $M_h^{[111]}$ versus temperature curves indicate the spin reorientation temperatures which depend on the intensity of the applied magnetic field. For magnetic fields equal to $H=0.2$, 1, and 2 T, we have the following values for spin reorientation temperatures: $T=52.6$, 44, and 36 K, respectively. It is worth noticing that the higher the magnetic-field intensity, the lower the spin reorientation temperature. This result is physically expected since the increase of the magnetic-field intensity in the [111] direction unbalances the anisotropy energy and a smaller amount of thermal energy (temperature) is necessary to liberate the magnetization vector, leading to alignment of the magnetization along the applied field.

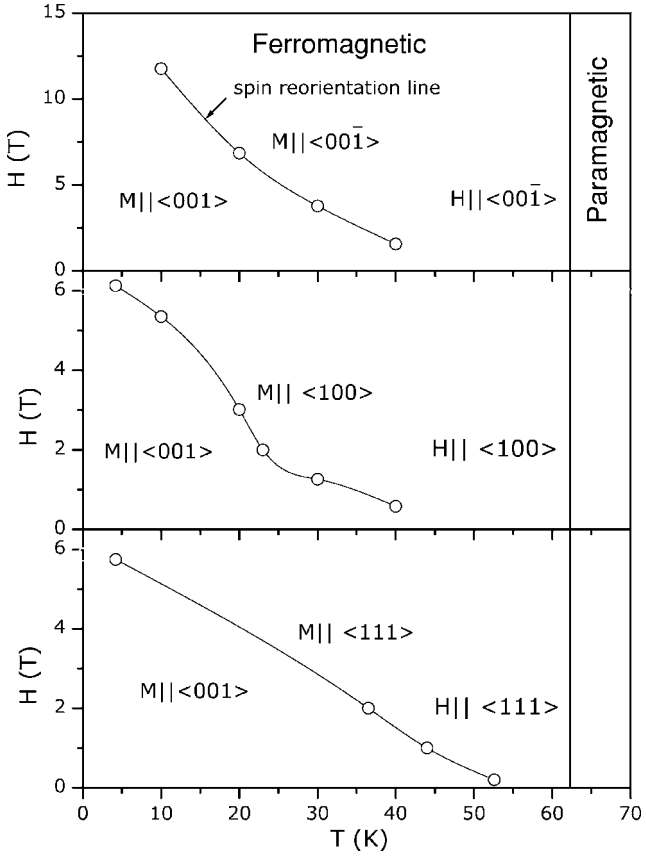

FIG. 9. (H vs T) magnetic phase diagram. Above the curves, the magnetic spin reorientation process is completed in the directions indicated. Below the curves, the magnetic system is in the easy magnetic direction. The points were obtained in this work and the solid curve is a guide for the eyes.

A detailed behavior of the temperature dependence of magnetization of $DyAl_2$ in zero field and in $H=2$ T applied in the [100] direction is displayed in Fig. 8. For zero magnetic field (dotted curve), we observe a continuous profile in comparison with the curve calculated with applied field (solid curve), which presents a strong discontinuity at spin reorientation transition. It should be noted the anomalous effect of the magnetic field which leads to lower values of the magnetization in the temperature interval $0<T<T_R$ compared to the magnetization values without magnetic field. Above T_R, a normal behavior is observed, i.e., the magnetization increases with magnetic field. The anomaly in the magnetization (order parameter) in the temperature interval $0<T<T_R$ will be reflected in the magnetic entropy. Inset (A) in Fig. 8 shows the magnetic entropy versus temperature calculated in $H=0$ T and $H=2$ T. For the temperature range $0<T<T_R$, the magnetic field increases the magnetic entropy (anomalous behavior for ferromagnetic system) in comparison with the magnetic entropy without the presence of the magnetic field. Above T_R, the magnetic entropy decreases under magnetic-field application (normal behavior in ferromagnetic system). We must bear in mind that this anomaly only occurs when the magnetic field is applied in a noneasy magnetic-field direction in such a way that the CEF anisotropy leads to the existence of a spin reorientation tempera-

ture. Inset (B) in Fig. 8 shows the temperature dependence of ΔS_{iso} under magnetic-field change from 0 to 2 T applied in the [100] direction. The anomalous negative values of ΔS_{iso} occur in the temperature interval where the spin reorientation process takes place, and the temperature where the ΔS_{iso} changes the signal is the reorientation temperature T_R.

Figure 9 shows the magnetic phase diagram. The points in the curves give the critical spin reorientation magnetic field and temperature obtained in this work, and the solid curves is a guide for the eyes. Below the curves, the magnetization vector is oriented along the easy magnetic direction [001] and above the curves the spin reorientation occurs in directions indicated in the figure.

IV. FINAL COMMENTS

In this paper, the conception of the anisotropic magnetocaloric effect was discussed and a quantitative description was introduced and applied to the ferromagnetic $DyAl_2$ compound. The anisotropic MCE in $DyAl_2$ comes from the CEF interaction which acts on the Dy localized magnetic moment and depends on the magnetic-moment orientation in the crystallographic referential frame. The magnetic state equation was obtained and solved using the three-dimensional mean-field self-consistent procedure. The theoretical model reproduces satisfactorily the experimental data of the temperature and magnetic-field dependencies of the magnetization when the magnetic field is applied in the [111] noneasy magnetic direction. A considerable isothermic entropy change of $\Delta S_{iso} \approx 2.8$ J/mol K for a fixed magnetic-field intensity of $H=1.5$ T (which can be obtained with a permanent magnetic device) was predicted to occur in $DyAl_2$—when the magnetic-field direction is changed from the easy magnetic direction to the $[00\bar{1}]$ direction. A possible construction of a magnetic refrigerator using the magnetic anisotropy effect of a $DyAlO_3$ single crystal was proposed by Kuz'min and Tishin.[26] In this device, the working body (refrigerant material), having the shape of a cylinder, turns around the cylinder axis in a fixed magnetic field and the rotation causes magnetization and/or demagnetization and consequently heating and/or cooling due to the MCE in a refrigeration cycle. The investigations in ΔT_{ad} as well as the experimental data on anisotropic MCE for $DyAl_2$ are being performed and will be published elsewhere. The studies of the CEF-anisotropy influence in magnetocaloric materials are just starting and may have an impact on experimental investigations in order to design magnetocaloric materials to be used as a refrigerants in magnetic refrigerators.

ACKNOWLEDGMENTS

We acknowledge financial support from CNPq, Conselho Nacional de Desenvolvimento Científico e Tecnológico, Brazil, Fundação de Amparo à Pesquisa do Estado do Rio de Janeiro (FAPERJ), and Coordenação de Aperfeiçoamento do Pessoal de Nível Superior (CAPES). This work was also partially supported by PRONEX No. E-26/171.168/2003 from FAPERJ/CNPq. We wish to thank Flavio C. G. Gandra for valuable comments about this work.

*Corresponding author.
Electronic address: vonranke@nitnet.com.br

[1] V. K. Pecharsky and K. A. Gschneidner, Jr., Phys. Rev. Lett. **78**, 4494 (1997).
[2] W. Choe, V. K. Pecharsky, A. O. Pecharsky, K. A. Gschneidner, Jr., V. G. Young, Jr., and G. J. Miller, Phys. Rev. Lett. **84**, 4617 (2000).
[3] Virgil Provenzano, Alexander J. Shapiro, and Robert D. Shull, Nature (London) **429**, 853 (2004).
[4] O. Tegus, E. Brück, K. H. J. Buschow, and F. R. de Boer, Nature (London) **415**, 150 (2002).
[5] H. Wada and Y. Tanabe, Appl. Phys. Lett. **79**, 3302 (2001).
[6] H. Wada, T. Morikawa, K. Taniguchi, T. Shibata, Y. Yamada, and Y. Akishige, Physica B **328**, 114 (2003).
[7] F. Hu, B. Shen, J. Sun, Z. Cheng, G. Rao, and X. Zhang, Appl. Phys. Lett. **78**, 3675 (2001).
[8] A. Fujita, S. Fujieda, Y. Hasegawa, and K. Fukamichi, Phys. Rev. B **67**, 104416 (2003).
[9] P. J. von Ranke, N. A. de Oliveira, and S. Gama, J. Magn. Magn. Mater. **277**, 78 (2004).
[10] P. J. von Ranke, N. A. de Campos, L. Caron, A. A. Coelho, S. Gama, and N. A. de Oliveira, Phys. Rev. B **70**, 094410 (2004).
[11] P. J. von Ranke, N. A. de Oliveira, and S. Gama, Phys. Lett. A **320**, 302 (2004).
[12] S. Gama, A. A. Coelho, A. de Campos, A. M. Carvalho, F. C. G. Gandra, P. J. von Ranke, and N. A. de Oliveira, Phys. Rev. Lett. **93**, 237202 (2004).
[13] P. J. von Ranke, N. A. de Oliveira, C. Mello, A. M. Carvalho, and S. Gama, Phys. Rev. B **71**, 054410 (2005).
[14] P. J. von Ranke, Sergio Gama, A. A. Coelho, A. de Campos, A. M. Carvalho, F. C. G. Gandra, and N. A. de Oliveira, Phys. Rev. B **73**, 014415 (2006).
[15] P. J. von Ranke, V. K. Pecharsky, K. A. Gschneidner, and B. J. Korte, Phys. Rev. B **58**, 14436 (1998).
[16] P. J. von Ranke, M. A. Mota, D. F. Grangeia, A. M. Carvalho, F. C. G. Gandra, A. A. Coelho, A. Caldas, N. A. de Oliveira, and S. Gama, Phys. Rev. B, **70**, 134428 (2004).
[17] A. L. Lima, I. S. Oliveira, A. M. Gomes, and P. J. von Ranke, Phys. Rev. B **65**, 172411 (2002).
[18] P. J. von Ranke, A. L. Lima, E. P. Nobrega, X. A. da Silva, A. P. Guimarães, and I. S. Oliveira, Phys. Rev. B **63**, 024422 (2000).
[19] A. L. Lima, A. O. Tsokol, K. A. Gschneidner, Jr., V. K. Pecharky, T. A. Lograsso, and D. L. Schlagel, Phys. Rev. B **72**, 024403 (2005).
[20] P. J. von Ranke, I. G. de Oliveira, A. P. Guimarães, and X. A. da Silva, Phys. Rev. B **61**, 447 (2000).
[21] P. Bak, J. Phys. C **7**, 4097 (1974).
[22] M. T. Hutchings., Solid State Phys. **16**, 227 (1964).
[23] K. R. Lea, M. J. M. Leask, and W. P. Wolf, J. Phys. Chem. Solids **33**, 1381 (1962).
[24] K. W. H. Stevens, Proc. Phys. Soc., London, Sect. A **65**, 209 (1952).
[25] H. G. Purwins and A. Leson, Adv. Phys. **39**, 309 (1990).
[26] M. D. Kuz'min and A. M. Tishin, J. Phys. D **24**, 2039 (1991).